On the effect of separated oxygen and carbon dioxide injections on the stabilisation of diluted oxyfuel flames

Sarah Juma, D. Honoré, B. Lecordier, Xavier Paubel, A. Cessou

INFUB - 11th European Conference on Industrial Furnaces and Boilers, INFUB-11

On the effect of separated oxygen and carbon dioxide injections on the stabilisation of diluted oxyfuel flames

S. Juma[1,2], D. Honoré[2*], B. Lecordier[2], X. Paubel[1], A. Cessou[2]

[1]Air Liquide CRCD Paris-Saclay, Les Loges en Josas, France

[2] CORIA - CNRS UMR 6614, Normandie Université, INSA Rouen Normandie, Université de Rouen Normandie Saint-Etienne du Rouvray, France

Abstract

Oxyfuel combustion with exhaust gas recycle coupled with CO_2 capture and storage (CCS) is a promising way to meet low CO_2 emission standards in industrial facilities with limited economical impact. In such systems, the flame stability is very sensitive to the dilution by injection of exhaust gases, particularly in configurations where they are not premixed with the oxygen, making the design of the burners more complex but offering a larger operation flexibility and a better control of flame heat transfer. In order to study the strategies of injection of the oxygen and exhaust gases, this paper presents an experimental study of the aerodynamic mechanisms influencing the stabilization of CO_2-diluted oxy-fuel flames, for four different configurations of 23 kW quadri-coaxial burners with separated injections for oxygen and carbon dioxide.
The four burners have same axisymmetric geometry consisting in injections of methane in the center surrounded successively by a first oxygen (O_{2i}) inner annular jet, the CO_2 co-flow and a second oxygen (O_{2e}) outer annular jet. Dimensions of burners are chosen to keep constant CH_4 and O_{2i} injections and to be able to change independently CO_2 and O_{2e} velocities for constant thermal power, total equivalence ratio, oxygen repartition and dilution ratio. The interaction between combustion and the aerodynamic features is investigated by CH* chemiluminescence imaging and Particle Image Velocimetry (PIV). Mean tomographic images of the flame structure are obtained by Abel's inversion of averaged chemiluminescence images. PIV measurements are performed for two fields of view in order to obtain the global aerodynamic features of the turbulent oxyfuel flames and a more precise characterization in the vicinity of the burner exit. For the latter, the spatial resolution of the measurements is optimized by the development of a specific multi-step PIV processing. Low flow-velocity and high flow-velocity configurations are tested at maximum CO_2 dilution allowed by the burners. Different structures of flames are obtained with a long continuous annular shape or with local extinction for some operating conditions. The intensity of the mixing processes and the resulting stability of the flame depend largely on the shear constraints between CO_2 and O_{2e} jets. A better stabilization is found for low CO_2 velocity, which favors its mixing with outer oxygen annular jet prior to direct dilution of the flame. An increase of O_{2e} velocity further improves centrifugal entrainment of CO_2 and then reduces the radial stratification around the flame. These results obtained in a reference configuration are useful guides for the design of flexible and efficient oxy-fuel industrial burners for CCS units.

Keywords: oxyfuel combustion ; diluted combustion ; Flue Gas Recirculation ; CCS

1. Introduction

The socioeconomic costs linked to CO_2 emissions in the atmosphere require the development of new technologies to control the environmental impact of combustion. Oxyfuel combustion produces fumes with high CO_2 content, ready for storage (CCS) or valorization (EOR) after purification at a lower cost compared to air-combustion products. It appears as a promising mean-term solution, as it is economically competitive and does not require new technological development [2]-[5].

The elimination of air nitrogen affects the thermal transfers when retrofitting industrial facilities originally designed for air-combustion. An exhaust gases recycle (EGR) loop must be set-up to replace the missing volume

* Corresponding author. Tel.: +33-232959852 ; fax: +33-232959780 .
E-mail address: david.honore@coria.fr

of nitrogen by exhaust gases, which allows the control of temperatures and thermal transfers as a function of the recycle rate. However, flame properties and stability are strongly influenced by the injection of exhaust gases with high CO_2 content, which inhibit the combustion [6]-[10]. The flame stability is increasingly challenged as the recycle rate rises. Therefore, the design of new burners adapted to oxy-fuel combustion with EGR and providing stable flames at high recycle rates is a major issue for the development of this technology.

The trend is to use existing air-burners and replace the air by a mixture of oxygen and exhaust gases. This method requires the cleansing of the exhaust gases to remove the unburned compounds prior to the mixing with oxygen within the burner. This operation is costly, and could likely favor the introduction of airborne nitrogen within the recycled flue gas, which may lead to the formation of NOx within the flame.

These drawbacks led to considering a new burner design based on the separation of the oxygen from the exhaust gases within the burner. However, this method may lead to stability issues due to separate injection of CO_2 which may act as a barrier between the fuel and the oxygen through stratification. The control of mixing processes is crucial to produce a homogeneous mixture and a stable flame, which is why the design of separate injection burners should be carefully led. The objective of the present work is to experimentally characterized these mixing processes and the corresponding diluted oxyflames with multi-coaxial burner configurations. This study is performed on a laboratory-scale facility by Particle Image Velocimetry to determine velocity fields at two different spatial resolutions and chemiluminescence imaging to obtain flame topology.

2. Experimental setup

For this purpose, an experimental study is performed with four 23 kW coaxial burners with separated injections for O_2 and CO_2, in a 1.20 meter-high and 40 cm diameter cylindrical lab-scale combustion facility [1]. The four quadri-coaxial ($CH_4/O_{2i}/CO_2/O_{2e}$) burners are based on a similar design (Figure 1). They are composed of a 4 mm-diameter (D) central injection of methane surrounded by a first coaxial injection of oxygen (O_{2i}). The next coaxial injection of carbon dioxide is surrounded by the last annular injection of secondary oxygen (O_{2e}). Carbon dioxide is injected between CH_4 and O_{2e} representing 90% of the total oxygen amount in order to guarantee a thorough dilution of CO_2 within the flame. The separation of CO_2 and O_{2e} injections promotes radial stratification of reactants dilution, which may destabilize the flame. The presence of internal oxygen injection O_{2i} is chosen to generate a central low intensity oxyflame attached to the burner. The variation of flow velocities of CO_2 and O_{2e} through changes of injection diameters d_3 and d_4 allows the study of the effect of mixing processes on the flame stabilisation. Two diameters d_3 and two diameters d_4 are considered, leading to four different burners providing independently either high or low CO_2 velocity, and either high or low O_{2e} velocity.

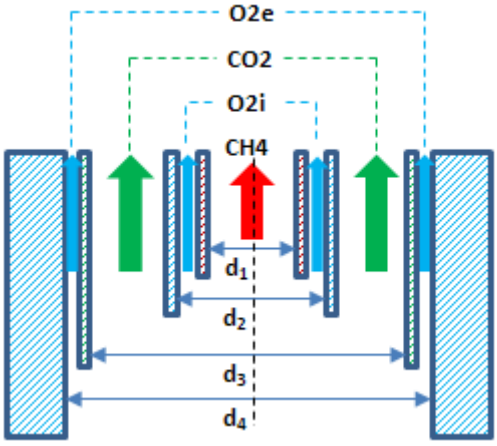

Figure 1 – General design of the burner.

The four different configurations of quadri-coaxial burners are tested on a combustion facility [11], consisting in a 1.20 m high and 0.40 m diameter cylindrical chamber. The thermal power is fixed at 23 kW and the global equivalence ratio φ at 0.98, guaranteeing approximately 2% O_2 within the flue gas.

The volumetric repartition of oxygen between the primary injection (O_{2i}) and the secondary injection (O_{2e}) is represented by parameter Ro. The dilution rate α is defined as the volumetric proportion of carbon dioxide in the "oxidant" O_2+CO_2. This study is held at Ro=10%, and at the maximum dilution rate allowed by the configuration – i.e. the maximum dilution rate for which a flame is stabilized.

The methane and the primary oxygen (O_{2i}) diameters and flow velocities are kept constant for the four burners C1-O1, C1-O2, C2-O1 and C2-O2, respectively in the order of 60 m/s and 15 m/s. The CO_2 and O_{2e} flow velocities are varied through d_3 and d_4, in order to identify aerodynamic effects favoring the stabilization of the flame for high dilution rates α. This induces a variation of the velocity ratio U_{O2}/U_{CO2} noted as r_2. The pipes thickness is 0.5 mm to avoid major bluff-body effects.

Table 1 – Outlets dimensions of the four burners

Burner	d_1 (mm)	d_2 (mm)	d_3 (mm)	d_4 (mm)
C1-O1	**4**	**6**	**9.46**	**11.8**
C1-O2				**14.0**
C2-O1			**18**	**19.8**
C2-O2				**21.2**

The combustion chamber wall is continuously cooled down by water circulating within a double stainless-steel casing. The water flowrate, inlet and outlet temperatures are controlled for thermal balance. The chamber is equipped with quartz optical windows (240x120 mm²) for chemiluminescence and PIV imaging. Eight thermocouples (penetrating 20 mm inside the chamber) and 5 fluxmeters are set on the chamber wall at different heights from the burner. A pressure probe is placed in the bottom of the chamber. A Siemens analysis unit with Ultramat 23 and Oxymat 61 analyzers records the mean dry flue gas concentrations (O_2, CO_2, CO, NOx and CH_4) after probing and cooling with an M&C® hot sampling line and cooler.

Mean flame structures are obtained from CH* chemiluminescence imaging by using a CCD camera (Roper Scientific Coolsnap 12 bits – 1300x1030 pixels) equipped with a 50 mm f/2.8 Nikon lens and a set of a BG12 band-pass and a GG375 high-pass filter. The axisymmetric configuration allows the reconstruction of the mean tomographic image by operating Abel's inversion on the obtained profiles [12]. The inverted images are normalized with respect to the longest exposure time, and to the highest intensity obtained for all the images.

The characterization of the velocity fields is achieved with a Particle Image Velocimetry (PIV) system [13]. The flows are seeded with dry ZrO_2 particles with a nominal diameter of 2 µm. The laser used is a double-pulse 200 mJ-15 Hz Nd-YAG Quantel laser operating at 532 nm. For high-resolution measurements at the burner nozzle, a 50 mm cylindrical lens and a 500 mm spherical lens are combined to perform a few centimeters high and a few-hundreds micrometers thick laser sheet, with maximum energy focused on the burner axis. The bottom of the laser sheet is cut with a sharp edge to avoid reflections on the burner surface. The measurement field size is 18x18 mm².The collection system is composed of a LaVision Imager ProX 14 bits camera equipped with an Infinity K2 microscope with its standard lens combination. A 532 nm interference filter is positioned in front of it to reduce the flame emission signal. The synchronization between the laser and the camera is achieved thanks to a programmable timing unit (PTU) and LaVision Davis 7.2 software, which is used for the collection of 300 pairs of images. The collection is realized with a 2 µs-delay between the laser pulses. The PIV correlation calculations are realized with a micro-PIV algorithm, adapted to the strong velocity gradients and low seeding behind the burner lips. This algorithm is based on the averaging of correlations, and leads directly to the mean-velocity field, through processing of the raw particle images obtained after background image subtraction. Because of the preferential flow direction, a rectangular meshing of the image is preferred, and two passes are applied with successive interrogation windows of 16x64 pixels and 6x12 pixels (eq. 0.06x0.12 mm²) with 1/3 overlap and window deformation. Intermediary validation steps consist in elimination of spurious vectors with displacement higher than 20 pixels, and a median filter over 3x3 pixels boxes. Instantaneous velocity fields are then calculated through an iterative two-steps FFT algorithm, with second-order mesh deformation, and with two passes for calculation and the mean-velocity field as an initial guess for the calculation. Final validation steps consist in elimination of spurious vectors with displacement higher than 20 pixels and a normalized median filter, adapted to strong velocity gradients, applied over 3x55 pixels boxes with parameter n=2 [14].

A global view of the mixing mechanisms further from the burner nozzle is provided by velocity measurements over large fields of view of 150x150 mm² above the burner. To provide these measurements, a cylindrical lenses combination resulting in 45 mm-focal-length, and a 750 mm-focal-length spherical lens, are combined to perform a constant-height laser sheet. The 150 mm diameter of the last spherical lens of this

periscope provides illumination for this large field of view. The camera is equipped with a Nikon 50 mm f/1.2 lens with an aperture of f/5.6 and a 532 nm interference filter. LaVision Davis 7.2 software is used for the collection and processing of the data. The PIV correlation calculations are realized with two passes in 32x32 pixels interrogation windows with 50% overlap and window deformation. The absence of peak-locking is checked, as well as the convergence of mean and rms values for the 300 images acquired. The post-processing includes elimination of spurious vectors by limiting the allowed vector range ($|u|<80$ m/s and $|v|<20$ m/s), a median filter, and validation with a peak ratio threshold $Q>1.3$. These processes are followed by vector interpolation. The velocity fields obtained are reliable for $x>D$, with a validation rate over 99% on average for all considered field and for all the burners.

The combination of the different fields of measurements provides reliable velocity data from $x=0$ to $x=37D$ even outside the flows thanks to the recirculation of seeded combustion products naturally occurring in the combustion chamber. The turbulent structures are well-resolved in the near-field up to $x=5D$, but more poorly-resolved for the 150x150 mm² field of view. For the latter, reliable fluctuation information is considered to be retrieved from $x=7D$.

3. Stability diagrams

For these four burners, the stability diagram is established as a function of Ro and dilution ratio α (Figure 2 and Figure 3). The limit of stability is defined at the extinction of flame or large CO emissions ([CO] > 400 ppm in flue gas).

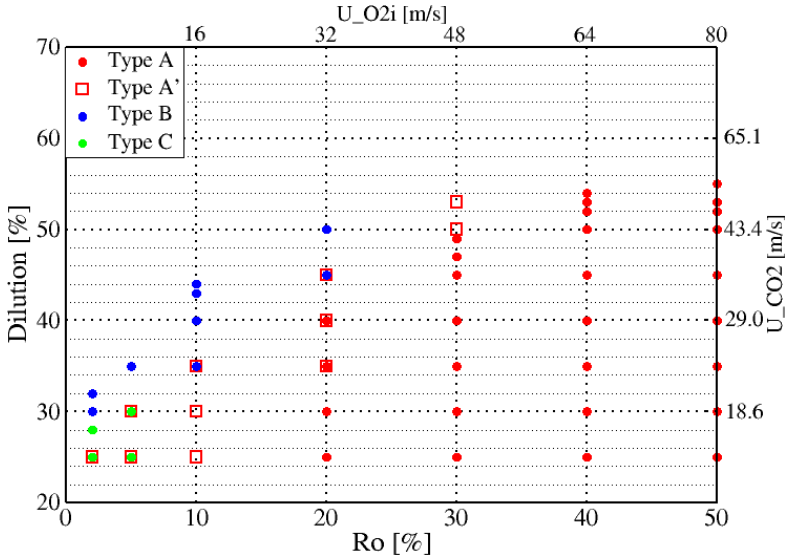

Figure 2 – Stability diagram for burners C1-O1 and C1-O2

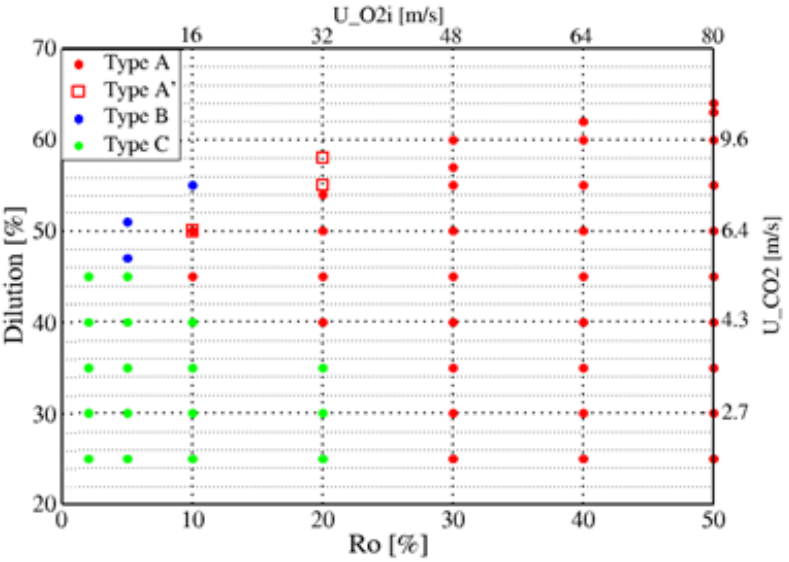

Figure 3 – Stability diagram for burners C2-O1 and C2-O2

Except for the limits of the stability diagrams, flue gas emissions for all stable flames show that the combustion is always complete in the flames with very low CO and NOx concentrations (< 10 ppm). Considering flames structures, four types of flame are identified depending on the operating conditions (Ro ; α), and are classified as type A, A', B and C.

Burner C2-O2 at (Ro = 50% ; α = 63%) illustrates type A flame on Figure 4.a, exhibiting a long continuous flame attached to the burner. The white bright flame at the burner outlet is due to the local high concentration of oxygen, and the blue color of the flame is explained by the high amount of CO_2. The distinctive feature for flame A (Figure 4– a) is the continuous decrease of CH* chemiluminescence that can be associated to a decrease of heat release from x=0 to the end of the visualization window.

Flame A' (Figure 4– b) is characterized by a noticeable separation of a primary combustion zone attached to the burner, and a secondary combustion zone, with the separation marked by a local minimum of heat release and thinner flame front. For burner C1-O1 at (Ro = 10% ; α = 30%), this local minimum is located at x=4D. Within the second combustion downstream x=4D, the heat release increases with a local maximum at x=12D before decreasing again downstream.

The flame from burner C2-O1 at (Ro = 5% ; α = 50%) is chosen to illustrate type B flame (Figure 4– c). Chemiluminescence mean image shows a primary combustion zone extending from x=0 (burner outlet) to x=10D. The absence of chemiluminescence signal from x=10D to x=28D reflects a long flame extinction, until the signal of chemiluminescence and the flame re-appear downstream x=28D. Type C flames therefore exhibit very distinctive features: a primary combustion zone and a secondary combustion zone clearly separated by a local extinction zone.

The type C flame (Figure 4– d) has a very specific shape and is characterized by a curved bulb-shaped flame. For C2-O1 burner at (Ro = 2% ; α = 25%), a primary combustion zone extends from x=0 to x=3D and expands towards the periphery, while a secondary combustion zone converges centripetally towards the longitudinal axis from x=3D to x=5D before expanding again.

All these flames exhibit a primary combustion zone, corresponding to the injection of oxygen around the methane, and a secondary combustion zone, associated to the mixing between the methane and the secondary oxygen surrounding the CO_2 injection. The distinctive features for each type are linked to the transition area between the primary flame and the secondary flame.

The goal of this study is to analyze the mixing mechanisms in order to explain the changes between the different flames types. The operating conditions for this detailed study is set at the maximum achievable dilution ratio α_{max} for Ro = 10%. The corresponding mean velocities for the fluids for each burner at these conditions are presented in Table 2.

Table 2 – Mean fluid velocities at burner outlets at the study defined operating points.

Burner	Ro (%)	α (%)	V_{CH4} (m/s)	V_{O2i} (m/s)	V_{CO2} (m/s)	V_{O2e} (m/s)	$r_2 = \frac{V_{O_{2e}}}{V_{co_2}}$
C1-O1	**10**	**44**	**53**	**16**	**34**	**18**	**0.5**
C1-O2						**53**	**1.6**
C2-O1		**50**			**6.5**	**18**	**2.8**
C2-O2						**51**	**7.7**

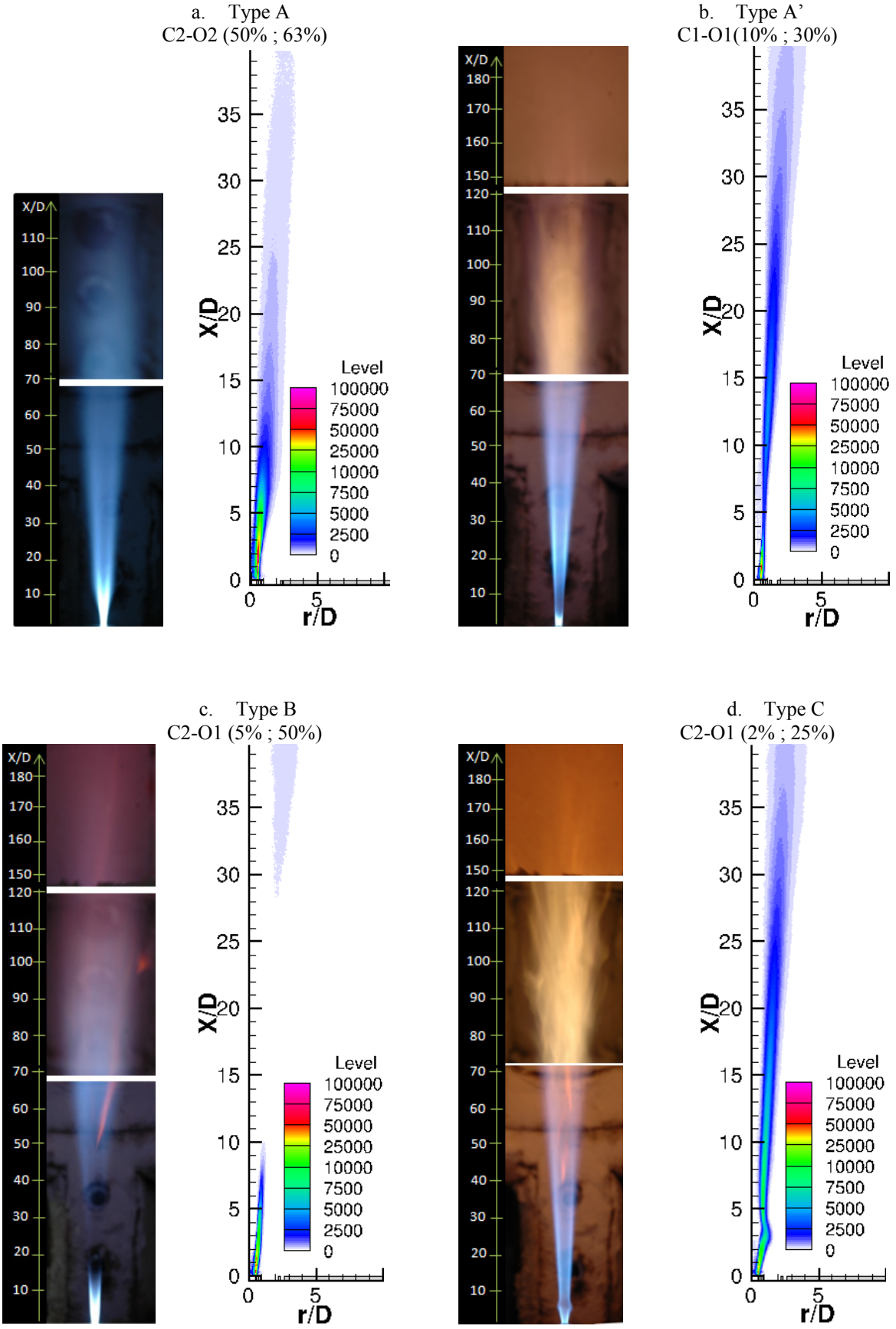

Figure 4 – Photographs and Abel's inversions for mean chemiluminescence image for A (image a), type A' (image b), type B (image c) and type C (image d) flames. The burner longitudinal axis corresponds to r=0. The chemiluminescence signal is given in arbitrary units.

4. Identification of mean flame structures

The objective is to identify the burner configuration which provides the more stable flame structure, and to identify the mixing mechanisms that pilot that structure. The mean flame structures are identified through CH* chemiluminescence for the four burners at (Ro=10% ; α_{max}). Figure 5 presents mean tomographic images obtained by Abel's inversion of averaged CH* chemiluminescence images.

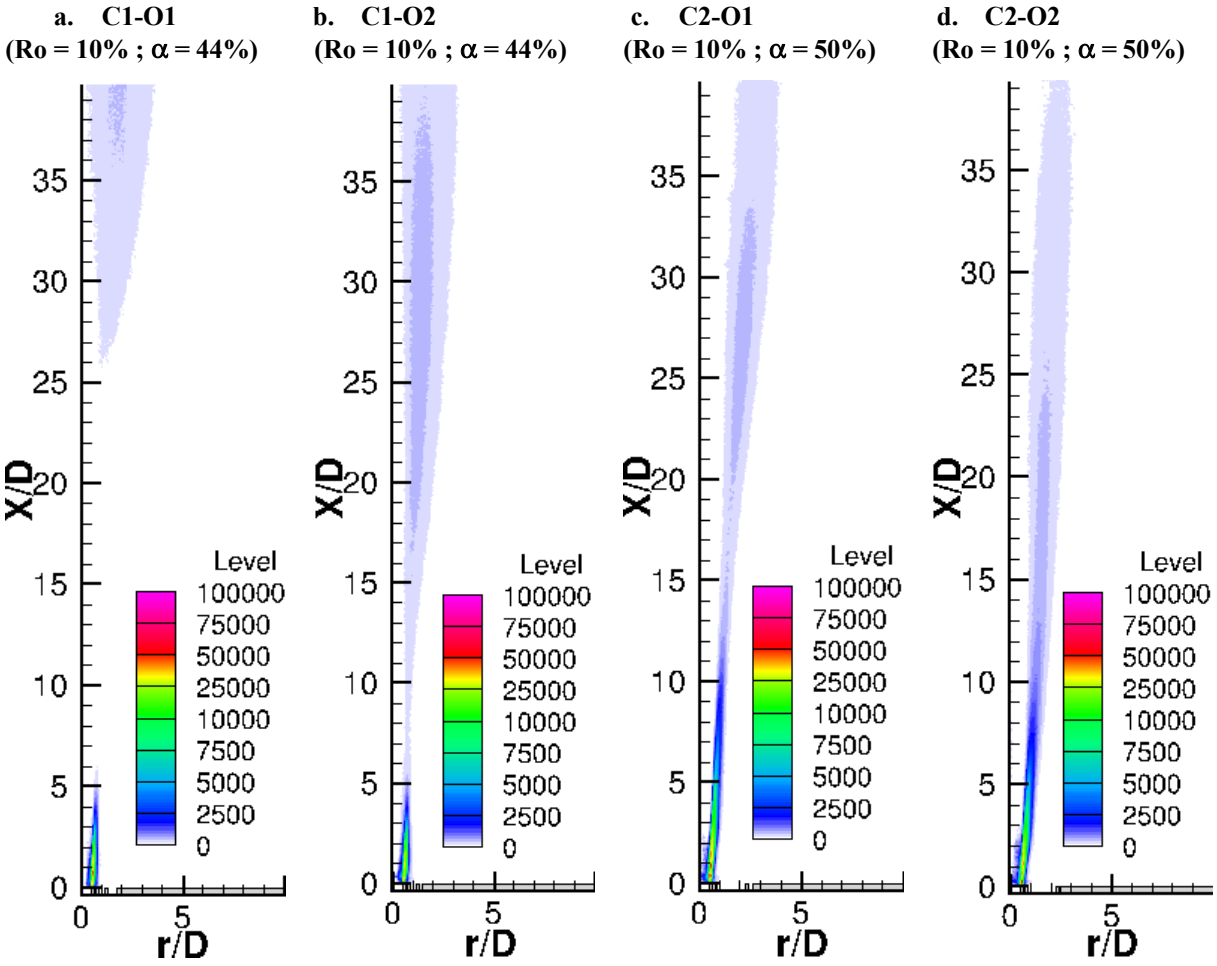

Figure 5 – Mean tomographic CH*chemiluminescence images obtained after Abel's inversion or the four burners at their maximal dilution rate for Ro=10%.

Burner C1-O1 is referred to as the "base case", with high CO_2 velocity and low O_{2e} velocity (Table 2). The flame obtained for these operating conditions is type B (Figure 5-a) with primary flame extending from x=0 to x=5D, and secondary flame base starting in the region of x=26D. The zone between x=5D and x=26D is a zone of local extinction in average. When O_{2e} velocity is higher, for burner C1-O2 (Figure 5-b), at same dilution rate α and same CO_2 velocity, (Table 2), the flame is type A' with local decrease of heat release between x=5D and x=15D. When CO_2 velocity is lower compared to the base case, for burner C2-O1, the flame is a type A' (Figure 5-c), with a minimum of heat release and thinner mean flame localized in the region between x=15D and x=20D. When CO_2 velocity is lower and O_{2e} velocity is higher compared to the base case, C2-O2 configuration produces a type A flame, for which heat release intensity decreases continuously from x=0, due to dilution of the flame by CO_2 and combustion products. The global stability of the flame appears even better than for the previous configurations. From these observations of mean flame structures, it seems the stability of the flame improves from base case a (C1-O1) to case d (C2-O2). As this improvement can be expected to be correlated to the mixing mechanisms, velocity fields measurements are performed by PIV (Figure 6) from the burner outlet. The velocity fields, superimposed with chemiluminescence contours of the flame, enable to locate the flame within the flow over a total length close to 40D.

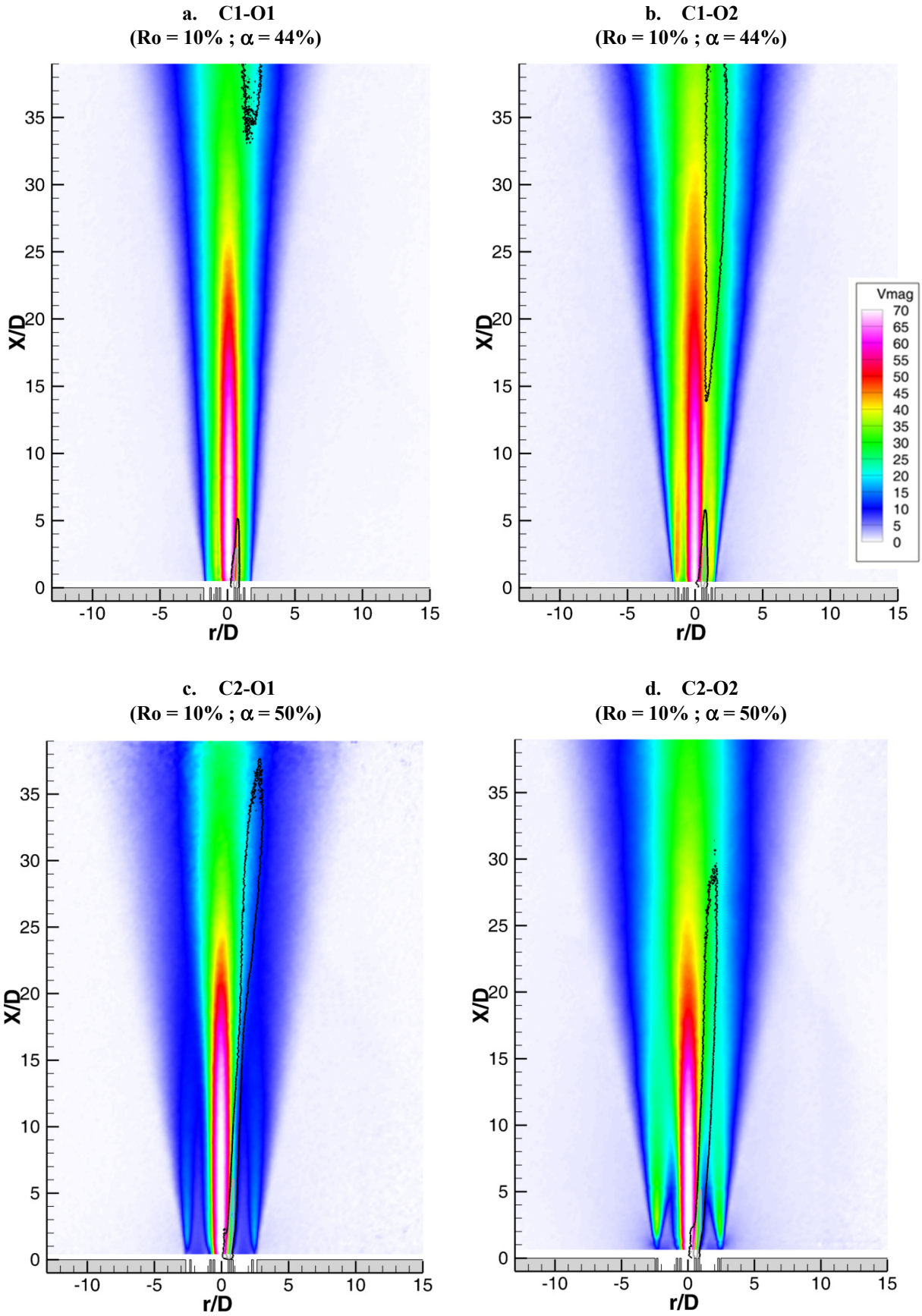

Figure 6 – Mean fields of velocity magnitude obtained through PIV. Mean contours of the flame obtained through Abel's inversion of mean CH* chemiluminescence image (at 300 and 5000 a.u.) are superimposed.

The primary flame is attached to the burner, between the methane and primary oxygen injections, and the secondary flame develops at the mixing interface between the central methane jet and the peripheral CO_2/O_{2e} mixture. The distinctive morphology for each flame is piloted by the mixing processes in the region of the nozzle exit. The spatial resolution of PIV measurements in such large field of view is not sufficient for a detailed description of the aerodynamics at the vicinity of the burner, as evidenced on Figure 6, and more particularly for C1-O2 and C2-O2 flame, where the O_{2e} exit velocity which is greater than 60 m/s, cannot be measured because of the small size of the injectors compared to the camera magnification ratio. For this purpose, a focus is made on the nozzle exit with a dedicated macro camera lens and a specific PIV algorithm. The resulting near-burner velocity fields, providing high spatial resolution, are studied comparatively for each burner (Figure 7 and Figure 8).

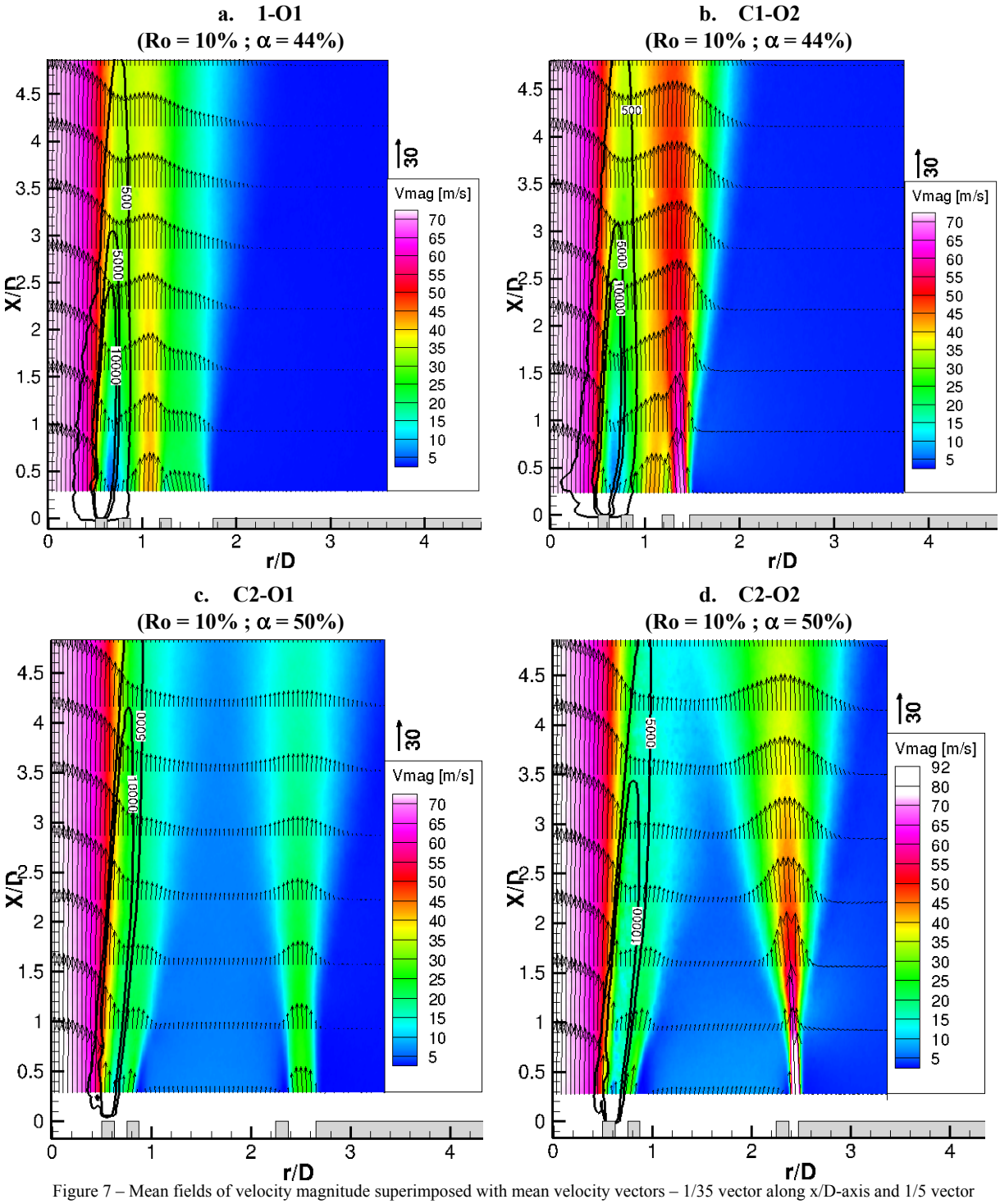

Figure 7 – Mean fields of velocity magnitude superimposed with mean velocity vectors – 1/35 vector along x/D-axis and 1/5 vector along r/D-axis – obtained through PIV in the near-field of the injector. Mean contours of the flame obtained through Abel's inversion of mean CH* chemiluminescence image (intensity in arbitrary units) are superimposed.

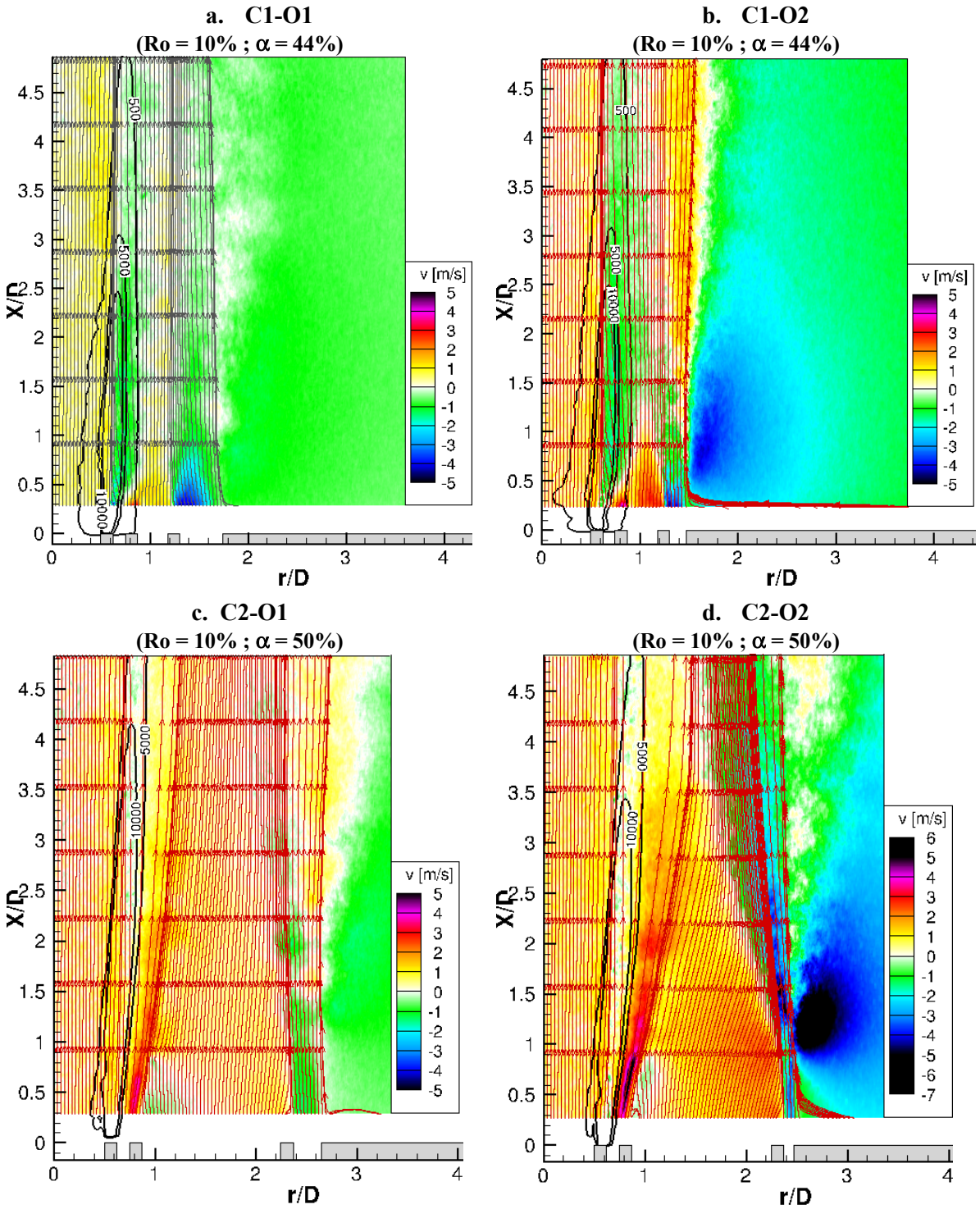

Figure 8 – Mean radial velocity field superimposed with streamlines and mean flame contours obtained through Abel's inversion of CH* chemiluminescence image for the four burners.

4.1. Stabilization mechanisms for high CO_2 and low O_{2e} injections velocities (C1-O1 case)

For the base case C1-O1, the flame is type B with a large extinction between 5D and 34D. In the near-field of the injector, the flame is clearly located behind the methane injection lip (Figure 7-a) at the interface between methane and O_{2i} [18], [19]. The development of the jets, characterized by the velocity fields, puts in evidence that the flow is mainly vertical and confined over the first diameters: the O_{2e} flows with low expansion towards the periphery. The coaxial configuration promotes radial stratification for the jets, which have to mix through radial transfer of momentum in order to stabilize the flame. This can be seen on the radial velocity fields presented Figure 8-a. The O_{2i} is confined at the interface between CO_2 and methane, and entrained by the latter,

as evidenced by the negative radial velocities, forming a strong primary flame. From x=4D, the mixture formed by O_{2i}, CO_2 and O_{2e} converges towards the center, which is evidenced by the centripetal velocities at this point. The CO_2 enters rapidly the flame causing the local extinction typical of this B flame. External oxygen is entrained by the faster CO_2 flow, and meets the methane jet downstream causing reactivation of the combustion.

4.2. Effect of external oxygen velocity on flame stabilization (C1-O2 case)

For C1-O2 operating conditions, the O_{2e} is injected at higher velocity than for C1-O1 ones (Figure 7-b). The O_{2e} jet flows towards the methane and transfers momentum towards the periphery, entraining burnt gases (Figure 8-b). Carbon dioxide is entrained by the O_{2e} flow towards the methane due to a velocity ratio r_2 higher than 1, which explains the weakening of the combustion zone, due to the interaction of the flame, with CO_2 and fresh gases, typical of type A' flame. As the O_{2e} converges faster towards the center, the mixing with methane occurs upstream compared to base case. The higher radial velocities (Figure 8-b) due to greater velocity gradients and jet entrainment explain the more efficient mixing between O_2 and CH_4.

The comparison between radial velocities fluctuations (Figure 9) highlights the presence of eddies which propagate from CO_2/O_{2e} interface and O_{2e}/burnt gases interface towards the reaction zone. It shows a better mixing for C1-O2 configuration due to the high O_{2e} velocity, which favors the momentum transfer and the mixing of O_2 and CH_4, thus enabling to obtain a type A' flame, with attachment of the secondary flame to the primary flame (case C1-O2) instead of a type B flame for C1-O1 operating conditions.

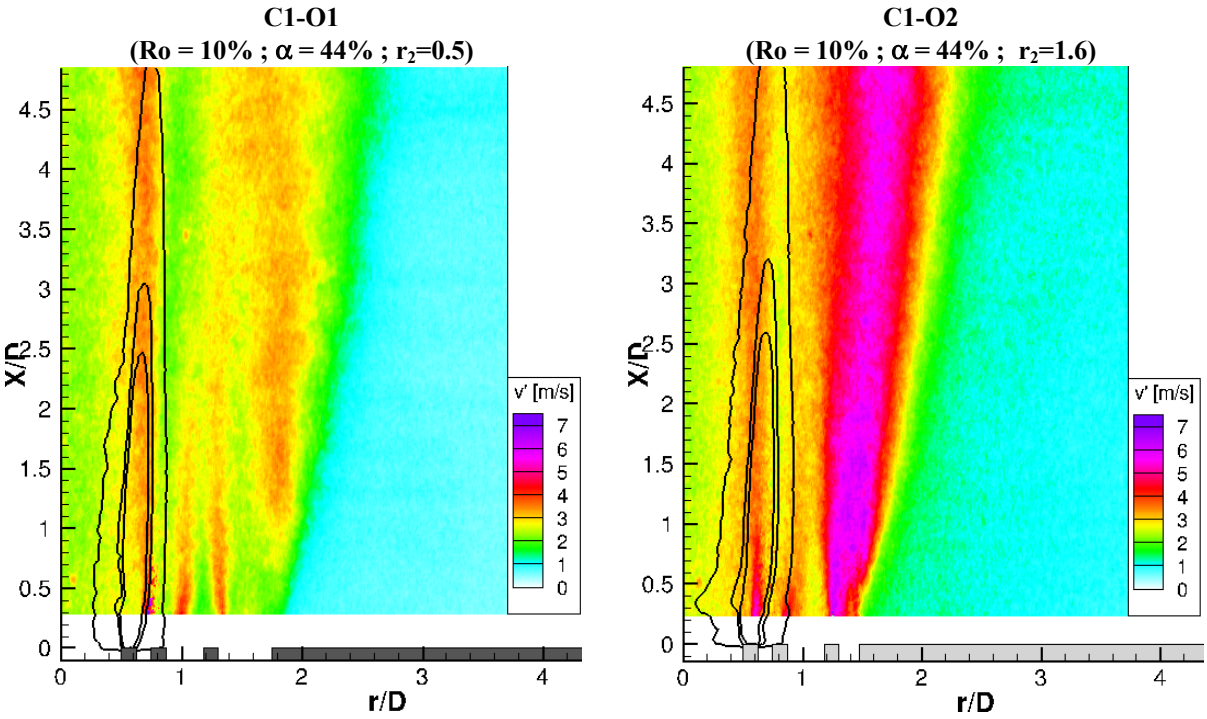

Figure 9 – Radial fluctuations v' fields superimposed to mean flame contours obtained through Abel's inversion of CH* chemiluminescence image (500, 5000 and 10000 a.u.) for burners C1-O1 and C1-O2.

4.3. Effect of carbon dioxide velocity on flame stabilization (C2-O1 case)

For C2-O1 flame, the CO_2 is injected at lower velocity than for C1-O1, which is induced by a wider injection surface, and for a close dilution ratio α=50%. The O_{2e} injection velocity is the same than the C1-O1 base case. The flame expands more towards the periphery than the base case, as shown by chemiluminescence contours (Figure 7-c). The confinement of the primary flame is broken as evidenced by the diverging streamlines close to the flame (Figure 8-c), which favors the expansion of the methane towards the periphery and mixing with the oxygen. This causes remoteness of CO_2 far from the reaction zone. Thus, with lower local dilution, a higher heat release is observed for the primary flame for this configuration compared to previous flames: the chemiluminescence contour for 10,000 a.u. extends up to x=4D, against approximately x=2.5D for burners C1-O1 and C1-O2.

The CO_2 stream is pinched between O_{2i} and O_{2e} (Figure 7-c) due to the local depression linked to the lower velocity of CO_2, favoring the mixing of the reactants, and thereby inducing the attachment of the secondary flame to the primary flame. This configuration emphasizes the stabilizing effects of the decrease of CO_2 velocity, which proves to be more efficient for flame stability in our configuration than increasing the velocity of O_{2e} at high CO_2 velocity.

4.4. Optimization of injections strategy for flame stabilization enhancement (C2-O2 case)

The configuration C2-O2 (Figure 7-d) combines low CO_2-velocity and high O_{2e} velocity, leading to a large velocity ratio ($r_2 = 7.7$). The attached flame expands again towards the periphery and is not confined at methane-O_{2i} interface, as shown by the CO_2 streamlines which diverge from the center (Figure 8-d). The primary oxygen jet expands towards the periphery with higher radial velocity (up to 6 m/s) than for burner C2-O1 (up to 4 m/s) (Figure 8-c and d). This effect, combined with the expansion due to the flame drives CO_2 away from the flame, favoring better stability of the flame. The secondary oxygen flow converges towards inner CO_2 jet with higher centripetal radial velocity (down to -6 m/s) than for burner C2-O1 (down to -2 m/s). This results in a stronger pinching of the CO_2 jet between higher-velocity O_{2i} and O_{2e} flows, which is characteristic of the local pressure decrease caused by high r_2 [20]. This fast merging between the two oxygen flows shortens the CO_2 potential core length to approximately 3D, and then enhances the mixing between carbon dioxide and oxygen.

The streamlines from O_{2i}, CO_2 and O_{2e} outlets tighten as the flows develop, emphasizing the increase of turbulent mixing mechanisms, which is consistent with the high velocity gradients generating high shear stress. Ultimately, the flame is type A with secondary flame directly attached to the primary flame, with no decrease of the combustion intensity thanks to the injection of O_{2e} in the combustion zone, balancing the CO_2 dilution in the flame.

High r_2 velocity ratio linked to C2-O1 and C2-O2 configurations promote high shear strain, which results in an efficient mixing of O_{2e} with CO_2 as observed on planar turbulent kinetic energy fields (Figure 10). The increase of r_2 induces shortenings of CO_2 and O_{2e} potential cores: their respective lengths decrease from 5D and 1.5D for burner C2-O1, to 2.5D and 0.5D for burner C2-O2. Moreover, for the latter case, the high kinetic energy, due to the high velocity gradients, enhances downstream mixing between the central CH_4 jet and (O_2 - CO_2) surrounding flow.

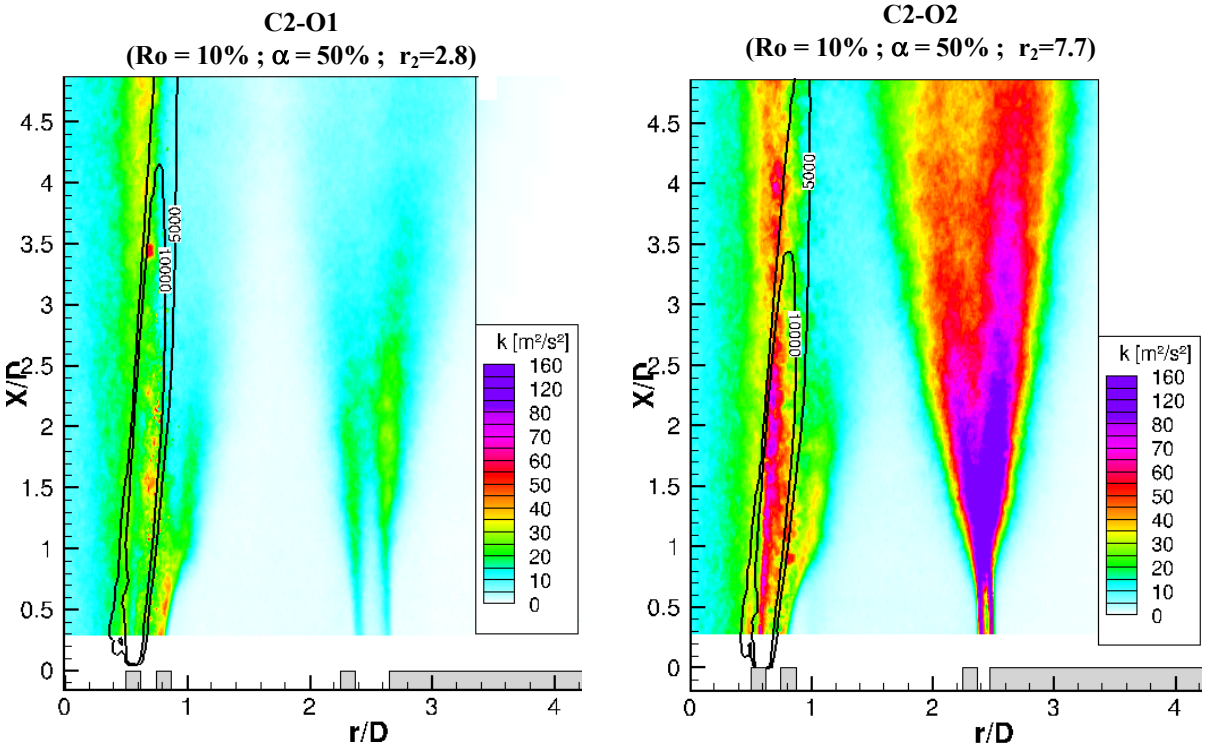

Figure 10 – Turbulent kinetic energy fields for C2-O1 and C2-O2 burners superimposed with mean flame contours.

These results put in evidence that the stability of the flame improves when O_{2e} velocity is increased and CO_2 velocity is lowered, due to mixing mechanisms improvement through velocity gradients. The importance of parameter r_2 in the stabilization process is underlined. In our studied configurations, CO_2 acts as a barrier

between CH_4 and O_{2e} which is the main source of oxidizer (Ro = 10%). The flame stability improves when radial stratification is lowered, due to the convergence of O_{2e} outer flow towards CH_4 central jet.

The influence of r_2 velocity ratio is also pointed out through the kinetic turbulent energy growth at the center of methane jet (Figure 11) for both C2-O1 and C2-O2 configurations, which are characteristic of an enhanced mixing. The methane potential core length is even shorter for burner C2-O2 (~11D) than for burner C2-O1 (~13D) which is characteristic of the faster convection by O_{2e} jet of the turbulent structures generated in the main shear layers and provides better stabilization for the flame. For both C2 configurations, linked to high r_2 due to the geometry of the injectors, the maximum attainable dilution rate is higher than for C1 configurations (Figure 12), where only lower r_2 are possible.

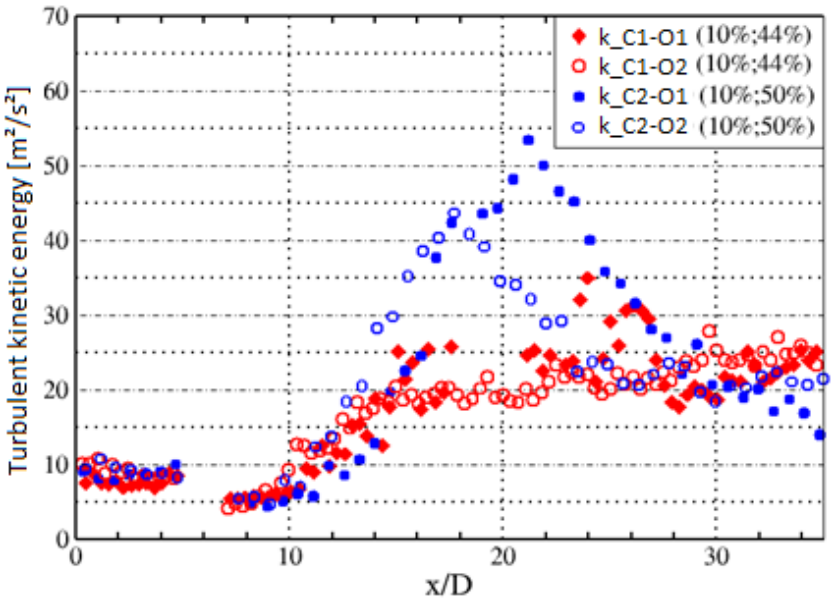

Figure 11 – Longitudinal evolutions of turbulent kinetic energy along the burner centerline for all configurations.

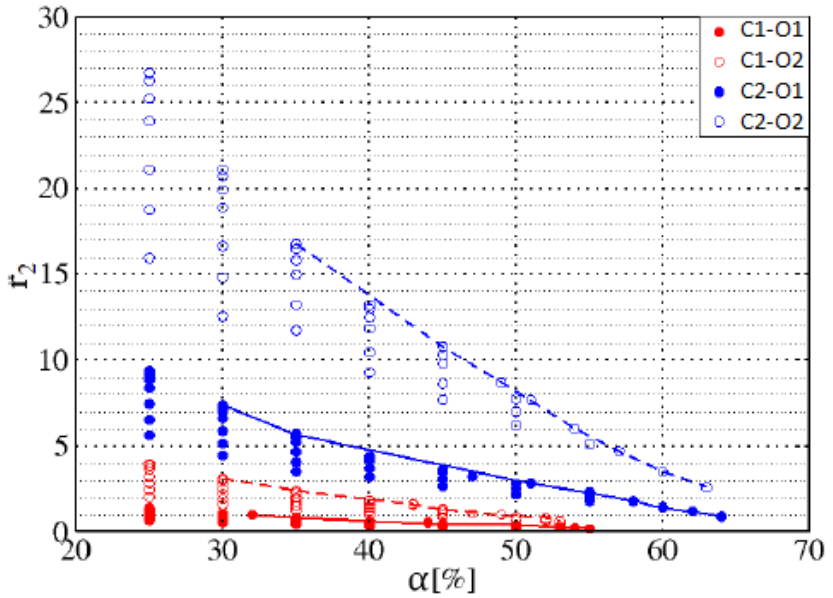

Figure 12 – Stability diagram for the four burners as a function of r_2 and α. The lines represent the critical operating conditions (α_{max} ; r_{2max}) where limits of flame stability are experimentally reached.

5. Conclusions

Four quadri-coaxial configurations of $CH_4/O_2/CO_2/O_2$ burners, with separated injections for CO_2 and O_2 have been investigated. The separation of carbon dioxide and oxygen injections in oxy-burners with recycling of exhaust gases offers a unique flexibility in terms of fuel nature and CO_2 dilution but may imply a stratification of

the flows which lead to flame instability in some configurations. The four different configurations give the opportunity to study the parameters controlling flame stability through modification of the mixing mechanisms of the reactants within the combustion chamber.

Due to the low tip thickness and large velocity gradients between the jets, the development of wake instabilities is moderate, and the mixing processes are mainly controlled by the development of turbulent structures at the interface between the jets. The intensity of the mixing processes and resulting stability of the flame are found to depend largely on shear constraints initiated by the velocity gradients between the co-annular flows of CO_2 and O_{2e}.

Two parameters are identified in order to control the mixing, and to balance the radial stratification of the flows and the destabilization of the reaction zone: the CO_2 velocity, and its comparison with O_{2e} velocity (r_2 ratio). In particular, it is shown that delaying the entrance of CO_2 within the flame (e.g. by lowering CO_2 velocity) and favoring the O_{2e} mixing with CO_2 and convergence of O_{2e} jet towards central fuel jet through high r_2 ratio and low CO_2 pressure tend to stabilize the flame and suppress the local extinction zones observed at high CO_2 velocity. The homogeneity of the mixing between O_2 and CO_2 is a necessary condition for flame stability, and to avoid stratification at the flame base when CO_2 dilution is increasing. These observations are useful guides for the design of flexible separated O_2/exhaust gases injection burners at industrial scale. Indeed, even if the present study is led at 23 kW with simple pipe-in-pipe configurations and voluntarily few stabilizing artefacts, it puts in evidence that separated injections of CO_2 and oxygen are possible, but require more complex configurations for industrial applications in order to reach higher dilution rates. Industrial burners are generally designed for power ranges in the order of 100 kW to several MW, and involve systems of swirls, thick walls that maximize bluff body effect for stabilizing the flame and multiple oriented injections. Such configurations would favor the mixing of the reactants and reduce the radial stratification between CO_2 and O_2 flows. According to this study, a burner configuration providing thick walls or swirls, low CO_2 velocity with injectors directed towards the periphery and high velocity O_2 directed towards a central natural gas jet, would be adapted to withstand higher dilution rates at higher power. Tests in a pilot facility of such designed burners could validate these guidelines and may be an intermediate step towards scale-up at industrial level.

References

[1] S. Juma – Oxycombustion diluted with CO_2: study of the strategy of injection of CO_2. *PhD Thesis,* Université de Rouen Normandie*,* 2014

[2] Chapel D., Ernest J., Mariz C. – Recovery of CO_2 from Flue Gases: Commercial Trends. *Annual Meeting of the Canadian Society of Chemical Engineers*, October 4-6, 1999, Canada

[3] Buhre B.J.P., Elliott L.K., Sheng C.D., Gupta R.P., Wall T.F. - Oxy-fuel combustion technology for coal-fired power generation. *Progress in Energy and Combustion Science*, vol. 31, 2005, pp. 283-307

[4] Singh D., Croiset E., Douglas P.L., Douglas M.A. – Techno-economic study of CO_2 capture from an existing coal-fired power plant: MEA scrubbing vs. O_2/CO_2 recycle combustion. *Energy Conversion and Management*, vol. 44, 2003, pp. 3073-3091

[5] Andersson K., Johnsson F. – Process evaluation of an 865 MW_e lignite-fired O_2/CO_2 power plant. *Energy Conversion and Management*, vol. 47, pp. 3487-3098, 2006

[6] Heil P., Toporov D., Forster M, Kneer R – Experimental investigation on the effect of O_2 and CO_2 on burning rates during oxyfuel combustion of methane. *Proceedings of the. Combustion Institute*, vol. 33, 2011, pp. 3407-3413,

[7] Glarborg P., Bentzen L.L.B. - Chemical effects of a high CO_2 concentration in oxy-fuel combustion of methane. *Energy and Fuels*, vol. 22, 2008, pp. 291-296

[8] Normann F., Andersson K., Leckner B., Johnsson F. - Emission control of nitrogen oxides in the oxy-fuel process. *Prog. Energy Combust. Sci.*, vol. 35, 2009, pp. 385-397

[9] Andersson K, Johnsson F. - Flame and radiation characteristics of gas-fired O2/CO_2 combustion. *Fuel*, vol. 86, 2007, pp. 656-668

[10] Oh J., Noh D. – The effect of CO_2 addition on the flame behavior of a non-premixed oxy-methane jet in a lab-scale furnace, *Fuel*, 2013, (http://dx.doi.org/10.1016.j.fuel.2013.08.065)

[11] Paubel X. - Analyse expérimentale des oxy-flammes turbulentes non prémélangées de gaz à faible pouvoir calorifique. *Thèse de doctorat*. INSA de Rouen, 2007

[12] Susset A. – Développement de traitements d'images pour l'étude de la stabilisation de flammes turbulentes non-prémélangées générées par des brûleurs industriels modèles. *Thèse de doctorat*. Université de Poitiers, 2002

[13] Boutier A. – Vélocimétrie laser pour la mécanique des fluides. *Hermes & Lavoisier*, 2012

[14] Westerweel J. – Efficient detection of spurious vectors in particle image velocimetry data sets. *Experiments in Fluids,* vol. 16, 1994, pp.236–247

[15] Overmars E.F.J., Warncke N.G.W., Poelma C., Westerweel J. – Bias errors in PIV: the pixel locking effect revisited. *15th Int Symp on Applications of Laser Techniques to Fluid Mechanics*, Lisbon, Portugal, 05-08 July, 2010

[16] Scarano F. – Iterative image deformation methods in PIV. *Meas. Sci Technol*., vol. 13 R1, 2002, doi:10.1088/0957-0233/13/1/201

[17] Westerweel J., Scarano F. – Universal outlier detection for PIV data. *Experiments in Fluids*, vol. 39, 2005, pp. 1096-1100

[18] Juniper M., Candel S. – Edge diffusion flame stabilization behind a step over liquid reactant. *Journal of Propulsion Power*, vol. 19, 2003, pp. 332-341

[19] Candel S., Juniper M., Singla G., Scouflaire P, Rolon C. – Structure and dynamics of cryogenic flames at supercritical pressure. *Combustion Science and Technology*, vol. 178, 2006, pp. 161-192

[20] Rehab H., Villermaux E., Hopfinger E.J. – Flow regimes of large-velocity-ratio coaxial jets. *Journal of Fluid Mechanics*, vol. 345, 1997, pp. 357-381